Available online at www.sciencedirect.com
ScienceDirect
Journal of Nuclear Materials 373 (2008) 387–401
journal of nuclear materials
www.elsevier.com/locate/jnucmat

Precipitation of the FeCu system: A critical review of atomic kinetic Monte Carlo simulations

E. Vincent [a,b], C.S. Becquart [a,*], C. Pareige [c], P. Pareige [c], C. Domain [a,b]

[a] Laboratoire de Métallurgie Physique et Génie des Matériaux, UMR 8517, Université de Lille 1, F-59655 Villeneuve d'Ascq cedex, France
[b] EDF R&D Département Matériaux et Mécanique des Composants, Les Renardières, F-77818 Moret sur Loing cedex, France
[c] Groupe de Physique des Matériaux, UMR CNRS 6634, Université de Rouen, Site du Madrillet, UFR Sciences, Avenue de l'Université BP 12, 76801 Saint Etienne du Rouvray, France

Received 15 February 2007; accepted 26 June 2007

Abstract

Cu is of primary importance in the embrittlement of the neutron-irradiated reactor pressure vessel (RPV) steels. It has been observed to segregate into copper-rich precipitates within the ferrite matrix under irradiation. Since its role was discovered more than 40 years ago, Cu precipitation in α-Fe has been studied extensively under irradiation as well as under thermal ageing using atom probe tomography, small angle neutron scattering, and high resolution transmission electron microscopy. Numerical simulation techniques such as Rate Theory or Monte Carlo methods have also been used to investigate this problem, however not always with a great success. In this paper, we provide a critical review of the different kinetic Monte Carlo models dedicated to the study of Cu precipitation, with the aim of determining which elements are key to an accurate description of precipitation.

PACS: 61.72.Ji; 61.80.−x; 71.20.Be; 71.15.Mb

1. Introduction

Cu is of primary importance in the embrittlement of the neutron-irradiated reactor pressure vessel (RPV) steels. Its role was put forward more than forty years ago [1]. Even if it is present in a very small amount, around 0.07 wt%, in the French RPV steels, the formation of Cu clusters has been observed thanks to characterisation techniques such as atom probe tomography (APT), small angle neutron scattering (SANS) and high resolution transmission electron microscopy (HRTEM). Cu precipitation has thus been studied exhaustively experimentally, both under thermal ageing and irradiation (electron, ion and neutron radiation). Despite the large amount of work about this alloy, the composition of the Cu clusters under neutron irradiation [2] is still very much debated. Indeed, with SANS and field emission scanning transmission electron microscopy, these clusters look like precipitates, containing close to 100% Cu [3,4], whereas with APT, they appear to be more or less dilute and are sometimes called 'atmospheres' [5–7] in the first stage of the precipitation. Thus, the decomposition of the FeCu system under irradiation appears complex, and the classical laws of thermodynamics cannot be applied in this context because of the point defect super saturation. On the other hand, under thermal ageing, the principles of thermodynamics can be applied. Furthermore, the studies indicate that Cu cluster formation takes place via the classical processes of nucleation, growth and coarsening. Finally, the results of APT and SANS converge to the same conclusion: Cu precipitates become rapidly almost pure [8,9]. This is the reason why the first numerical simulations of Cu precipitation were concerned with the study of thermal ageing, the other reason being that thermal ageing is simpler to simulate than radiation.

Different methods can be used to model precipitation kinetics at the atomistic level. One class of models relies

* Corresponding author.
E-mail address: charlotte.becquart@univ-lille1.fr (C.S. Becquart).

0022-3115/$ - see front matter © 2007 Elsevier B.V. All rights reserved.
doi:10.1016/j.jnucmat.2007.06.016

on cluster dynamics as in [10,11]. The other models are based on Monte Carlo (MC) type algorithms [12–15]. The later class is more appropriate to investigate the different mechanisms involved, while cluster dynamics allow to simulate large volumes and longer times.

In this paper, we focus on the precipitation of Cu under thermal ageing, and on its simulations using kinetic Monte Carlo (KMC) models. Indeed, being able to simulate correctly the precipitation of the FeCu system is the first and necessary step towards the prediction of the microstructural evolution of more complex alloys like ternary or quaternary alloys, not to mention alloys of pressure vessel steels.

Several KMC models [12–15] have been used to study the precipitation of the iron–copper system. The main differences between these are the method used to determine the vacancy activation energy, and the parameterisation. One possible approach [12–14] is based on a cut bond model in which the vacancy activation energy is given by the difference between the energy at the saddle point position and the energy due to the interactions of the bonds broken during the jump. The differences between these cut bond models are the parameterisations used. The other kind of model published is based on the calculation of the total system energies before and after the vacancy jump to determine the vacancy activation energy [15]. In all the models, the alloy cohesive energy is obtained as a sum of pair interactions. Among the groups using cut bond models, Soisson et al. [12] have compared the simulated precipitation kinetics in the FeCu system to experimental results of thermal ageing and electron irradiation, the only effect of electron irradiation being, according to these authors, the enhancement of the diffusion. They observe that under thermal ageing, the simulated system follows the classical law of Lifshitz–Slyozov–Wagner (LSW) [16,17]. Schmauder and Binkele [14] have proposed another model with which they follow the precipitate mean radius evolution in FeCu alloys aged at different successive temperatures. Le Bouar and Soisson [13] have studied the dependence of the activation energy with the local atomic configuration on the diffusion mechanisms in the FeCu system. They found that this dependence is important even in dilute alloys.

In the first part of the paper, the KMC theory will be briefly discussed, along with the different approaches used so far. In a second part, a parametric study of the influence of the various parameters on the kinetics, will be presented in order to determine which properties need to be included in the model to correctly reproduce Cu precipitation in α-Fe. Finally, we will compare the ability of the different models to simulate the ageing of an Fe-0.6at.%Cu alloy at 500 °C and of an Fe–1.4 wt%Cu alloy at 500 and 600 °C. Care has been taken in this work to systematically compare the simulated results to experimental ones (in terms of size and number density of particles). Note that in contrast to the clusters formed experimentally under thermal ageing, which contain, at least at the beginning of the treatment, some Fe atoms (according to APT), the precipitates simulated here are pure Cu precipitates.

2. Methodology

2.1. Ab initio calculations

Some properties, such as the binding or mixing energies used in the parameterisation, have been obtained by ab initio calculations. Our calculations have been done using the Vienna Ab initio Simulation Package VASP [18,19]. They were performed in a plane-wave basis, using fully non-local Vanderbilt-type ultrasoft pseudopotentials to describe the electron–ion interaction. Exchange and correlation were described by the Perdew–Zunger functional, adding a non-local correction in the form of the generalised gradient approximation (GGA) of Perdew and coworkers (PW91). All the calculations were done in the spin polarised GGA using the supercell approach with periodic boundary conditions. The ultrasoft pseudopotentials used in this work come from the VASP library. Brillouin zone (BZ) sampling was performed using the Monkhorst–Pack scheme. The defect calculations were done at constant volume, thus relaxing only the atomic position in a supercell dimensioned with the equilibrium lattice parameter for Fe (0.28544 nm). The plane-wave cut-off energy was 240 eV. Except when mentioned, the results are obtained using 128-atom supercells with a BZ sampling of $27k$ points. More details on the method and, in particular, a comparison of full relaxation versus constant volume calculations for defects in α-Fe can be found in a previous work [20].

The binding energy between two entities, A and B, in a bcc iron matrix containing N atomic sites, is calculated as follows:

$$E_b(A,B) = [E(N-1+A) + E(N-1+B)] - [E(N-2+A+B) + E_{ref}], \quad (1)$$

where $E(N-1+A)$ is the energy of a supercell containing only a defect A, $E(N-1+B)$ the energy of the same supercell containing only a defect B, $E(N-2+A+B)$ the energy of the same supercell containing A and B and E_{ref} the energy of the supercell containing no defect. In this scheme, a positive binding energy indicates an attractive interaction.

The mixing energy, corresponding to an infinite dissolution of Cu in bcc Fe, is determined as follows:

$$E_{mix}(\mathrm{Cu} \rightarrow \mathrm{Fe}) = [E((N-1)\mathrm{Fe} + \mathrm{Cu})_{bcc} - ((N-1)/N)E_{ref} - E(\mathrm{Cu}_{ref})], \quad (2)$$

where $E((N-1)\mathrm{Fe}+\mathrm{Cu})_{bcc}$ is the energy of a supercell containing $(N-1)$Fe atoms and one Cu atom, E_{ref} is the energy of a supercell containing N Fe atoms and $E(\mathrm{Cu}_{ref})$ is the cohesive energy of Cu in the faced cubic centred structure.

In this work, the set of ab initio data is divided into a fitting and a testing database as will be explained later.

2.2. Monte Carlo models

All the simulations presented in this paper as well as in [12–14] rely on the residence time algorithm derived by Young and Elcock [21] to model the diffusion of a vacancy in FeCu. In this kind of simulation, the vacancy diffusion is determined by the calculation of the eight (bcc lattice) probabilities of first nearest neighbour jumps. This probability is given by the following equation:

$$\Gamma_{X,V} = \nu_X \exp\left(-\frac{E_a}{kT}\right), \tag{3}$$

ν_X is the attempt frequency for the entity X (X = Fe, Cu), which makes an exchange with the vacancy and E_a is the activation energy of the jump. For each parameterisation presented here, the Cu attempt frequency has been taken equal to the Fe one. Its value is 6×10^{12} s^{-1} in our parameterisation, 3.65×10^{15} s^{-1} for [12,13] and it is 8.7×10^{12} s^{-1} for [14].

One of the key ingredient of the KMC methods is the determination of the activation energy. For all the methods presented in this paper, the cohesive model, necessary to determine the system energy, is described using pair interactions in a rigid lattice. The system is either described using pair interactions between first nearest neighbours only [12,13,22] or considering also the second nearest ones like in [14,23] and in our parameterisation. The knowledge of the pair interactions ε_{XX} between all the X entities (Fe, Cu or vacancy: V) which compose the system is necessary to obtain the total energy E of the system, which is then obtained as follows:

$$\begin{aligned} E = {} & N^{(i)}_{Fe\text{–}Fe}\varepsilon^{(i)}_{(Fe\text{–}Fe)} + N^{(i)}_{Fe\text{–}V}\varepsilon^{(i)}_{(Fe\text{–}V)} + N^{(i)}_{Fe\text{–}Cu}\varepsilon^{(i)}_{(Fe\text{–}Cu)} \\ & + N^{(i)}_{V\text{–}Cu}\varepsilon^{(i)}_{(V\text{–}Cu)} + N^{(i)}_{Cu\text{–}Cu}\varepsilon^{(i)}_{(Cu\text{–}Cu)}, \end{aligned} \tag{4}$$

where i equals 1 or 2 and corresponds respectively to first or second nearest neighbour interaction, $N^{(i)}_{Fe\text{–}Fe}$ is the number of Fe–Fe bonds, $N^{(i)}_{Fe\text{–}V}$ the number of Fe–V bonds, $N^{(i)}_{Fe\text{–}Cu}$ the number of Fe–Cu bonds, $N^{(i)}_{V\text{–}Cu}$ the number of V–Cu bonds and $N^{(i)}_{Cu\text{–}Cu}$ the number of Cu–Cu bonds of the lattice.

The activation energy E_a can be determined by various approaches. The three methods existing so far are described in the next paragraphs.

2.2.1. Model used in this work

The code used in this work is the LAKIMOCA code developed at EDF [15] [24]. In this model the activation energy is obtained from the final E_f and the initial E_i system energy (FISE) as follows:

$$E_a = E_{a_0} + \frac{E_f - E_i}{2}, \tag{5}$$

where E_{a_0} depends only on the migrating atom type: it is the ab initio vacancy migration energy in pure Fe when the vacancy jumps towards an Fe atom and it is the ab initio solute migration energy when the vacancy jumps towards a solute atom. E_i and E_f are estimated using Eq. (4) with first and second nearest neighbour pair interactions obtained from ab initio calculations. Eq. (5) satisfies the detailed balance rule. Note that the system total energy could have been obtained from empirical potentials as in [15,25]. However our final goal is to model complex alloys, containing solute atoms of more than one kind, for which realistic interatomic potentials are very tedious to build.

The pair interactions between copper atoms or between iron atoms are related to the cohesive energies of pure bcc copper and iron respectively as follows:

$$E_{coh}(X) = 4\varepsilon^{(1)}_{(X\text{–}X)} + 3\varepsilon^{(2)}_{(X\text{–}X)}, \tag{6}$$

where X stands for copper or iron. The pair interactions between an iron and a copper atom are obtained from the mixing energy and the interface energy along the (1 0 0) plane according to the two equations below:

$$\begin{aligned} E_{mix}(Cu \rightarrow Fe) = {} & -4\varepsilon^{(1)}_{(Fe\text{–}Fe)} - 3\varepsilon^{(2)}_{(Fe\text{–}Fe)} + 8\varepsilon^{(1)}_{(Fe\text{–}Cu)} \\ & + 6\varepsilon^{(2)}_{(Fe\text{–}Cu)} - 4\varepsilon^{(1)}_{(Cu\text{–}Cu)} - 3\varepsilon^{(2)}_{(Cu\text{–}Cu)}, \end{aligned} \tag{7}$$

$$\begin{aligned} E_{int(100)}(Fe/Cu) = {} & -2\varepsilon^{(1)}_{(Fe\text{–}Fe)} - \varepsilon^{(2)}_{(Fe\text{–}Fe)} + 4\varepsilon^{(1)}_{(Fe\text{–}Cu)} \\ & + 2\varepsilon^{(2)}_{(Fe\text{–}Cu)} - 2\varepsilon^{(1)}_{(Cu\text{–}Cu)} - \varepsilon^{(2)}_{(Cu\text{–}Cu)}. \end{aligned} \tag{8}$$

The vacancy–Cu and vacancy–Fe pair interactions are estimated from the first nearest neighbour vacancy–Cu binding energy and from the vacancy formation energies in bcc Cu and in bcc Fe respectively, as follows:

$$E^{(1)}_b(V\text{–}Cu) = \varepsilon^{(1)}_{(Fe\text{–}Cu)} + \varepsilon^{(1)}_{(Fe\text{–}V)} - \varepsilon^{(1)}_{(Fe\text{–}Fe)} - \varepsilon^{(1)}_{(V\text{–}Cu)}, \tag{9}$$

$$E_{for}(V^X) = 8\varepsilon^{(1)}_{(X\text{–}V)} + 6\varepsilon^{(2)}_{(X\text{–}V)} - 4\varepsilon^{(1)}_{(X\text{–}X)} - 3\varepsilon^{(2)}_{(X\text{–}X)}, \tag{10}$$

where X stands for copper or iron.

The absolute energies obtained with the VASP code (as in many other ab initio codes) usually have to be rescaled to be comparable to experimental cohesive energies. To rescale the Cu cohesive energy for the bcc structure, the energy difference between the most stable (the face centred cubic (fcc)) phase and the bcc phase has been calculated by ab initio and added to the experimental cohesive energy [26]. For iron, the cohesive energy used is the experimental one [26]. The interface energy (Eq. (8)) has been obtained with a 10-atom supercell and $10\times10\times1k$ points. As Cu is not stable in the bcc structure, it was not possible to perform ab initio calculations to obtain the relaxed vacancy formation energy in pure bcc Cu. This value was then adjusted. The fitting values, used in Eqs. (6)–(10), appear in Table 1 and the pair interactions deduced from them in Table 2. A testing database is also shown in Table 1 (data in bold characters). These testing data are energies which have not been used in the determination of the pair interactions but which can be calculated once the pair interactions have been obtained. They are compared to

Table 1
Fitting and testing (bold characters) parameters used in this work as well as in the works of Schmauder and Binkele [14], Soisson et al. [12] and Le Bouar and Soisson [13]

Model	FISE and CBM2	CBM1 [12]	CBM1 [13]	CBM1 [14]
E_{mig}(Fe) (eV)	0.62	1.23	0.638	0.903
E_{mig}(Cu) (eV)	0.54	0.55	0.208	0.895
E_{coh}(Fe) (eV)	−4.28	−4.28	−4.28	−4.28
E_{coh}(Cu)	−3.49	−4.28	**−3.84**	−4.28
$E_b^{(1)}$(Cu–Cu) (eV)	**0.07**	**0.18**	0.2	**0.094**
$E_b^{(2)}$(Cu–Cu) (eV)	**0.08**	**0**	**0**	**0.046**
$E_b^{(1)}$(V–Cu) (eV)	0.07	**0.04**	0.19	**0.047**
$E_b^{(2)}$(V–Cu) (eV)	**0.06**	**0**	**0**	**0.023**
$E_{for}(V^{Fe})$ (eV)	2.0	1.64	1.632	1.6
$E_{for}(V^{Cu})$ (eV)	1.6	2.04	**0.912**	1.6
E_{mix}(Cu → Fe) (eV)	0.5	0.72	0.8	0.515
E_{int}(1 0 0) (mJ/m^2)	407	**697**	**775**	**453**
E_{int}(1 1 0) (mJ/m^2)	**397**	**493**	**548**	**384**

the results of ab initio calculations, which allows us to obtain a first assessment of the validity of the pair interactions obtained. In our parameterisation, the (1 1 0) interface energy, the Cu–Cu binding energies, the second nearest neighbour V–Cu binding energy are testing energies. They can be obtained from the pair interactions as follows:

$$E_{int(110)}(\mathrm{Fe/Cu}) = -\varepsilon^{(1)}_{(\mathrm{Fe\text{–}Fe})} - \varepsilon^{(2)}_{(\mathrm{Fe\text{–}Fe})} + 2\varepsilon^{(1)}_{(\mathrm{Fe\text{–}Cu})} + 2\varepsilon^{(2)}_{(\mathrm{Fe\text{–}Cu})} - \varepsilon^{(1)}_{(\mathrm{Cu\text{–}Cu})} - \varepsilon^{(2)}_{(\mathrm{Cu\text{–}Cu})}, \quad (11)$$

$$E_{int(110)}(\mathrm{Fe/Cu}) = 2E_b^{(1)}(\mathrm{Cu\text{–}Cu}) + 2E_b^{(2)}(\mathrm{Cu\text{–}Cu}), \quad (12)$$

$$E_b^{(i)}(\mathrm{Cu\text{–}Cu}) = 2\varepsilon^{(i)}_{(\mathrm{Fe\text{–}Cu})} - \varepsilon^{(i)}_{(\mathrm{Fe\text{–}Fe})} - \varepsilon^{(i)}_{(\mathrm{Cu\text{–}Cu})}, \quad (13)$$

$$E_b^{(2)}(\mathrm{V\text{–}Cu}) = \varepsilon^{(2)}_{(\mathrm{Fe\text{–}Cu})} + \varepsilon^{(2)}_{(\mathrm{Fe\text{–}V})} - \varepsilon^{(2)}_{(\mathrm{Fe\text{–}Fe})} - \varepsilon^{(2)}_{(\mathrm{V\text{–}Cu})}. \quad (14)$$

More details about the validity of the ab initio values and about the parameterisation scheme are presented in [27].

2.2.2. Cut bond models

As written previously, the activation energy can also be determined using a cut bond model. With the model used in [12,22,13,14] referred later to as CBM1, the activation energy is the energy increase observed when moving an atom i, nearest neighbour of the vacancy, from its initial position (a stable lattice site) to the saddle point position. The activation energy is obtained as follows:

$$E_a = e_k^{sp} - \sum_j \varepsilon_{k-j} - \sum_{j\neq k} \varepsilon_{V-j}, \quad (15)$$

where e_k^{sp} is the binding energy of the atom k at the saddle point position and where the summations over j extend over all the broken bonds of the migrating atom k and of the vacancy. For the models presented here, e_k^{sp} is independent of the local environment. Note that, for the model of Le Bouar and Soisson [13], we used the value obtained independently from the local environment so as to be able to compare equivalent models. For [12,14], the pair interactions are estimated from the cohesive energies of pure metals (Eq. (6) up to, respectively, 1nn and 2nn interactions), the mixing energy (Eq. (7) up to, respectively, 1nn and 2nn interactions) and the vacancy formation energies in pure metals (Eq. (10) up to, respectively, 1nn and 2nn interactions). For Le Bouar and Soisson [13], the pair interactions are obtained from the Fe cohesive energy (Eq. (6) with only 1nn interactions), the vacancy formation energy in bcc Fe (Eq. (10) with only 1nn interactions), the mixing energy (Eq. (7) with only 1nn interactions), the first nearest neighbour vacancy–Cu binding energy (Eq. (9)) and also with the Cu–Cu binding energy (Eq. (13)). These energies can be experimental values [12], a mixing of experimental and fitting values [14] or values obtained from an empirical interatomic potential [13]. All the fitting values have been collected in Table 1, along with the testing data which appear in bold characters. The corresponding pair interactions are given in Table 2. More details can be found in [12–14].

We have developed another form of cut bond model which will be later referred to as CBM2. In this method, we consider that the migrating atom jump does not lead to the destruction of the bonds with the vacancy as in CBM1 but that the bonds between the migrating atom and its neighbours are replaced by bonds with a vacancy and the same neighbours (i.e. we explicitly take into account the fact that the migrating atom leaves a vacancy where it originally sat). The activation energy is then given by

Table 2
Pair interactions obtained for each parameter set (eV)

Pair interactions	$\varepsilon^{(1)}_{(\mathrm{Fe\text{–}Fe})}$	$\varepsilon^{(2)}_{(\mathrm{Fe\text{–}Fe})}$	$\varepsilon^{(1)}_{(\mathrm{Fe\text{–}V})}$	$\varepsilon^{(2)}_{(\mathrm{Fe\text{–}V})}$	$\varepsilon^{(1)}_{(\mathrm{Fe\text{–}Cu})}$	$\varepsilon^{(2)}_{(\mathrm{Fe\text{–}Cu})}$	e^{sp}_{Fe}
This work	−0.611	−0.611	−0.163	−0.163	−0.480	−0.571	−9.166[a]
Soisson et al. [12]	−1.070	–	−0.330	–	−0.980	–	−8.9
Le Bouar and Soisson [13]	−1.070	–	−0.331	–	−0.915	–	−9.5
Schmauder and Binkele [14]	−0.778	−0.389	−0.335	0	−0.731	−0.366	−9.557
	$\varepsilon^{(1)}_{(\mathrm{Cu\text{–}Cu})}$	$\varepsilon^{(2)}_{(\mathrm{Cu\text{–}Cu})}$	$\varepsilon^{(1)}_{(\mathrm{V\text{–}Cu})}$	$\varepsilon^{(2)}_{(\mathrm{V\text{–}Cu})}$			e^{sp}_{Cu}
This work	−0.414	−0.611	−0.102	−0.180			−7.266[a]
Soisson et al. [12]	−1.070	–	−0.280	–			−8.9
Le Bouar and Soisson [13]	−0.96	–	−0.366	–			−8.88
Schmauder and Binkele [14]	−0.778	−0.389	−0.335	0			−9.098

[a] Used with the CBM2 model only.

$$E_a = \sum_j \varepsilon^{sp}_{k-j} + \sum_j \varepsilon_{V-j} - \sum_j \varepsilon_{k-j}, \quad (16)$$

where $\sum_j \varepsilon^{sp}_{k-j}$ is the sum of the six pair interactions of the migrating atom k at the saddle point position, $\sum_j \varepsilon_{k-j}$ the sum of the first and second nearest neighbour pair interactions of the migrating atom k in its initial stable position and $\sum_j \varepsilon_{V-j}$ the sum of the first and second nearest neighbour pair interactions of the vacancy, replacing the migrating atom. The pair interactions (Table 2) are obtained from the same ab initio energies (Table 1) and consequently the same equations than those used in the FISE method. In our simulations, $\varepsilon^{sp}_{Fe-Cu} = \varepsilon^{sp}_{Fe-Fe} = e^{sp}_{Fe}$ and $\varepsilon^{sp}_{Cu-Cu} = \varepsilon^{sp}_{Cu-Fe} = e^{sp}_{Cu}$ in Table 2.

This new cut bond model was developed in order to describe differently the saddle point position and to test this effect on the vacancy migration. The migration energies obtained with these approaches are not correlated to the thermodynamics of the system like in the FISE model. They will thus enable us to assess and quantify the effect of the migration path on the evolution of the microstructure. The two cut bond models are illustrated in Fig. 1.

From a thermodynamic point of view, the essential parameters that should influence the precipitation are the driving force and the interface energies. In the KMC models, the mixing and the interface energies should thus be the determining parameters of the precipitation. From a kinetic point of view, the migration energies as a function of the local environment and in particular the diffusion coefficients play a key role. Great differences exist for the mixing energy from one set of parameters to another (Table 1). The solubility limits of the FeCu system therefore change from one model to another leading to very different driving forces. Using the Metropolis algorithm [28], we have determined the solubility limits at 500 °C (this temperature is that of the experimental thermal ageing we chose to model) corresponding to the four different values of the mixing energy. The definition of the solid solution is given in Section 3.2.1. The solubility limit equals 0.001 at.% with Le Bouar and Soisson [13] parameterisation, 0.002 at.% with that of Soisson et al. [12], 0.05 at.% with that of Schmauder and Binkele [14] and 0.07 at.% with our parameters. The two first values are very low and far from the experimental value estimated to be 0.1 at.% [29]. The corresponding driving forces for the precipitation are therefore high, which should lead to the formation of a high density of small Cu precipitates.

3. Results and discussion

Many experiments are available to study thermal ageing [9,29–32]. We will focus on the thermal ageing of an Fe–0.6 at.%Cu binary alloy at 500 °C, which we investigated using APT to obtain the evolution kinetics of the cluster mean radius and the cluster density. The recent work of Perez et al. [29] has also been used to complete the study and assess the temperature effect. We will thus compare the MC results to these two sets of experiments which we will describe briefly in the next paragraph.

3.1. Experimental results

We have studied the thermal ageing at 500 °C of a dilute FeCu alloy containing 0.6 at.% Cu by APT. The Cu cluster mean radius has been measured during thermal ageing up to 20 h (Fig. 2). Three different stages are observed. (i) During the nucleation stage, the precipitation of copper gives rise to Cu-atmospheres. (ii) During the growth stage, the mean radius grows with a time law close to the classical time law $t^{1/2}$ (Fig. 2) [33]. From this stage, Cu precipitates present a copper-rich core. (iii) Finally, during the coarsening stage, the cluster mean radius time evolution can be fitted by the classical $t^{1/3}$ LSW law [16,17] (Fig. 2). During this later stage, the number density of precipitates is expected to decrease. In our experiment (0.6 at.% Cu, 500 °C) it decreases after 1 h of ageing. This gives an experimental evidence that growth and coarsening occur simultaneously, as observed in numerous alloys. The particle number density varies from 3×10^{23} m^{-3} to 1×10^{23} m^{-3} (Fig. 2).

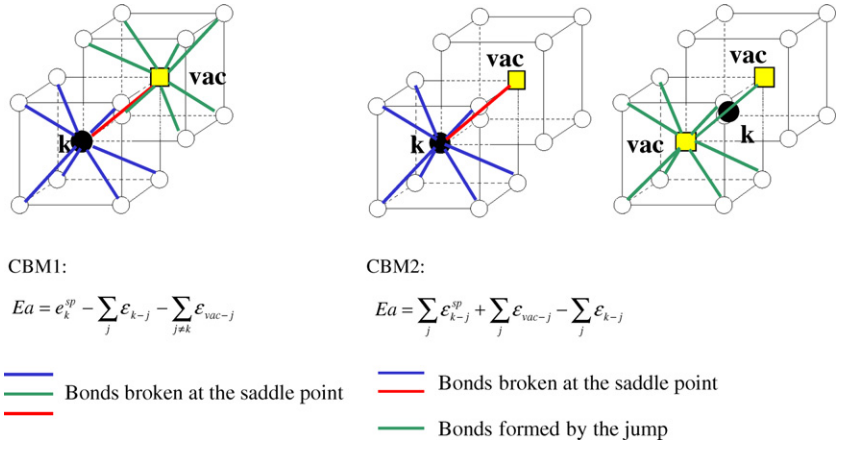

Fig. 1. Illustration of the two cut bond models.

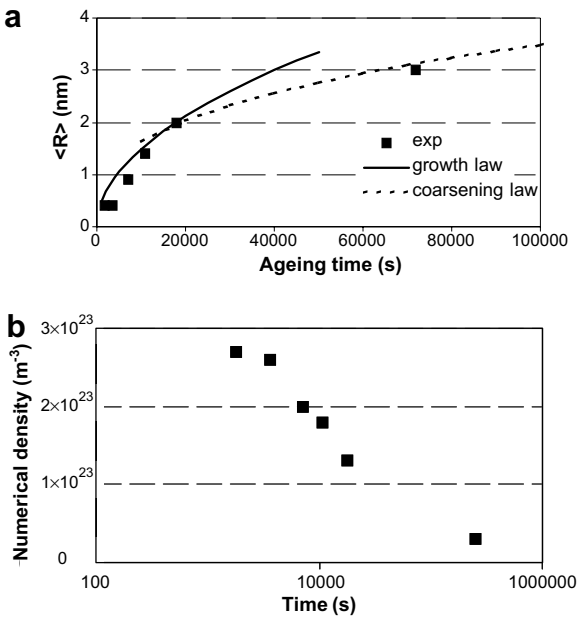

Fig. 2. Microstructure evolutions measured by APT versus ageing time for an Fe–0.6 at.%Cu alloy aged at 500 °C. (a) Mean particle radius of copper precipitates evolution. The plain curve represents the classical $t^{1/2}$ growth law. The dashed curve represents the LSW [16,17] coarsening law. (b) Numerical density of copper precipitates evolution.

Perez et al. [29] have thermally aged an Fe–1.4 wt%Cu alloy at 500 and 600 °C. Using small angle X-ray scattering (SAXS), they have measured the evolution kinetics of the Cu cluster mean radius during coarsening. The curves are shown in Fig. 3(a). According to the LSW theory [16,17], the growth exponent is close to 1/3. It is well known [34–37] that the Cu precipitates undergo structural changes going from the bcc structure to a 9R, then 3R and finally fcc structure. Depending on the authors, the precipitates lose their bcc structure when their radius reaches a size of 6 nm [35] 4.2 nm [37] or 5 nm [9]. As our simulations are performed on a rigid lattice, such transformations cannot be reproduced, as whatever their size, the precipitates in our model will remain bcc. For this reason, only the experimental data for which the precipitate sizes were small enough for them to be bcc have been used in the comparison.

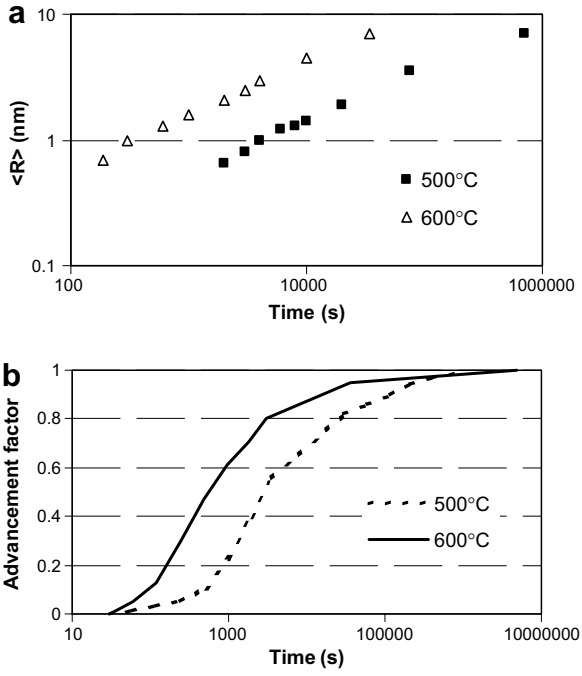

Fig. 3. Reproduction of the results of Perez et al. [29] obtained on an Fe–1.4 wt%Cu alloy aged at 500 °C and 600 °C. (a) Mean particle radius of copper precipitates as measured by SAXS versus ageing time; (b) advancement factor as measured by TEP and SAXS versus ageing time.

The precipitation advancement factor was another property measured by thermoelectric power (TEP) and SAXS. The two evolutions are given in Fig. 3(b). For Cu, it is given by the ratio of the Cu concentration in clusters at a given time over Cu concentration in clusters at infinite time. The relation used is thus

$$\zeta(t) = \frac{C_{\mathrm{Cu}}(0) - C_{\mathrm{Cu}}(t)}{C_{\mathrm{Cu}}(0) - C_{\mathrm{Cu}}(\infty)}, \tag{17}$$

where $C_{\mathrm{Cu}}(t)$ is the Cu concentration in the solid solution at time t, which tends towards the solubility limit $C_{\mathrm{Cu}}(\infty)$.

3.2. Simulation results: influence of the parameters and the models

The fitting parameters, chosen for our FISE model and used to solve Eqs. (6)–(10) are collected in Table 1. The influence of the value of these parameters will be discussed next with the FISE model.

Before studying the influence of the parameters on the precipitation, the definition of the solid solution as well as the method used to correlate simulated time and physical time should be specified.

3.2.1. Preliminary study

3.2.1.1. Characterisation of the solid solution. To simulate a solid solution, the solute atoms are randomly introduced in the simulation box. Thus, small Cu clusters containing a few atoms are formed, whose size depends on the Cu concentration. With a Cu concentration of 0.6 at.%, Cu clusters containing up to three atoms are formed when the Cu distribution is randomly distributed in the simulation box. As a consequence, all along the paper, for this alloy, clusters containing as many as three Cu atoms will be considered to belong to the solid solution. In the Fe–1.4 wt% Cu alloy, Cu clusters containing up to four atoms are initially present in the simulation box when the Cu atoms are randomly distributed. Therefore, for this alloy, we consider that a Cu atom which belongs to a cluster of four or less atoms is still part of the solid solution. A Cu atom belongs to a cluster if at least one of its first neighbour is also a Cu atom.

3.2.1.2. Determination of the Monte Carlo time. In each model presented, the residence time algorithm is applied [21]. MC time is thus incremented for each MC step by the following amount t_{MC}:

$$t_{MC} = \frac{1}{\sum_{i=1}^{8} \Gamma^{i}_{X-V}}, \tag{18}$$

where Γ^{i}_{X-V} is the jump probability of vacancy V towards one of the 8 atoms i.

Ageing is simulated by the introduction of one vacancy in the bcc lattice. During thermal ageing, the vacancy can be trapped in the copper precipitates as seen in Fig. 4. The amount of trapping depends on the parameterisation characteristics. To take this effect into account, the MC time is incremented only when the vacancy is in the matrix, as proposed by Le bouar and Soisson [13]. To determine whether the vacancy is in the matrix or in the precipitate, a comparative study has been performed by investigating the evolution kinetics of the Cu precipitate mean radius during the simulation of a thermal ageing of an Fe–0.6 at.%Cu at 500 °C. We followed the evolution of the Cu precipitate radius with time when the time is incremented whatever the vacancy environment, or when the time is not incremented as soon as the vacancy is surrounded by at least two or four Cu atoms. The three curves obtained were similar during the nucleation phase, which indicates (as expected) that during this phase, the vacancy is almost never surrounded by more than one Cu atom. However, during the growth phase, the curve obtained when the time is incremented at each MC step differed from the other two. This demonstrates that trapping takes place and needs to be accounted for. It was also observed that the number of Cu atoms close to the vacancy that we chose for not incrementing the time (in this case two or four) did not change the evolution kinetics. It was then decided to not increment the time when at least two Cu atoms surround the vacancy.

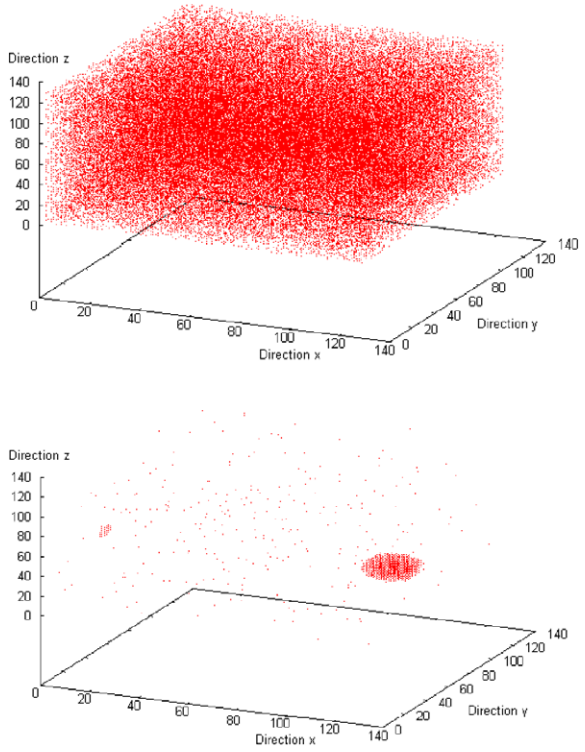

Fig. 4. Illustration of the trapping of the vacancy by a Cu precipitate. The dots represent the position of the vacancy during the simulation. Top figure: top the vacancy has explored the whole simulation box. Bottom figure: the vacancy has been trapped by a Cu precipitate.

One vacancy in a 64 unit cell simulation box corresponds to a very high vacancy concentration (2×10^{-6} at. fraction) compared to the experimental equilibrium vacancy concentration (between 10^{-13} and 10^{-11} at. fraction). To take that effect into account, the MC time has to be rescaled. Usually, the following equation is used [12]:

$$t = \left(\frac{C_{V,sim}}{C_{V,real}}\right) t_{MC}. \tag{19}$$

To determine the value of $C_{V,real}$, one can consider that the FeCu system is so diluted in Cu that it can be assimilated to a pure Fe system. In this case, $C_{V,real}$ is given by the relation:

$$C_{V,real} = \exp\left(-\frac{E_{for}(V^{Fe})}{kT}\right). \tag{20}$$

If one wishes to take into account the composition of the FeCu alloy, the value of $C_{V,real}$ can then be estimated from the relation:

$$C_{V,real} = \exp\left(-\frac{E_{for}(V^{Fe})}{kT}\right) \exp\left(\frac{\Delta S}{k}\right) \times \left[1 - 8x_{Cu} - 6x_{Cu} + 8x_{Cu} \exp\left(\frac{E_b^{(1)}(V\text{–}Cu)}{kT}\right) + 6x_{Cu} \exp\left(\frac{E_b^{(2)}(V\text{–}Cu)}{kT}\right)\right]. \tag{21}$$

where x_{Cu} is the solute Cu concentration, $E_b^{(1)}(V\text{–}Cu)$ and $E_b^{(2)}(V\text{–}Cu)$ are the vacancy–copper binding energies respectively in first and second nearest neighbour. Mathon [38] estimated $\frac{\Delta S}{k}$ to 2 for the Fe–Cu system. However, none of these equations enabled us to rescale time in a satisfying manner, leading us to think that none of the evaluations of the vacancy formation energy in the Fe–Cu system is accurate enough. In a first approximation, it was thus decided to adjust directly the MC time on the experimental one. For the simulated results obtained for one MC time, one looks for the experimental microstructure which is the closest to the simulated one. A multiplying factor is then estimated from the ratio of the real (experimental) ageing time over the simulated ageing time. This multiplying factor is then applied all along the simulation to obtain a physical time from the MC time. The advantages of this method are that it enables one to directly compare the different precipitation kinetics obtained with each method and each parameterisation, and that it allows one to see

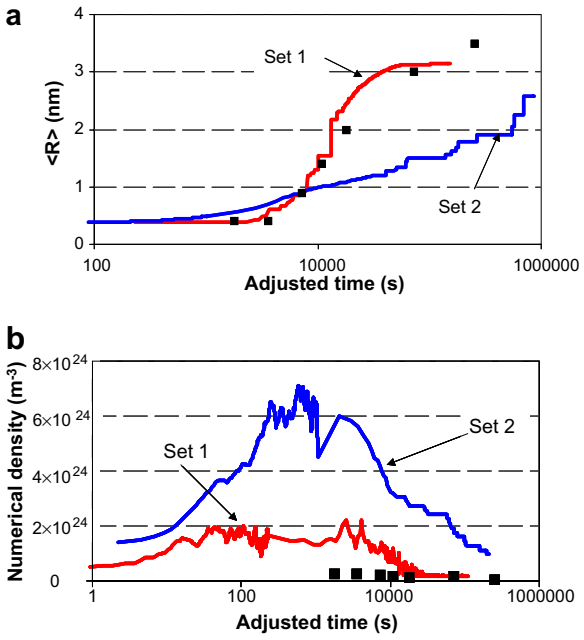

Fig. 5. Comparison of the kinetics obtained with two different values of the mixing energy. The black filled squares are the experimental data. (a) Evolution of the Cu cluster mean radius. (b) Evolution of the numerical density of the Cu clusters. One cluster in the simulation box corresponds to a numerical density of 1.6×10^{23} m^{-3}.

if the precipitation tendency agrees with experiments. An example is given in Fig. 5, where the MC time was adjusted when the cluster mean radius was equal to 0.9 nm. This corresponded to 7200 s of experimental thermal ageing. Note that this method is not entirely satisfactory either, as experimental results are needed to rescale the time.

Note that when several temperatures are studied, time is rescaled first with the Eqs. (19) and (21) in order to take into account the temperature effect on the value of the vacancy formation energy in the FeCu alloy. The time obtained is then directly adjusted on the experimental one.

3.2.1.3. Box size. Each ageing simulation has been performed in a simulation box which contains 64 unit cells in each of the three space directions. The box size should be high enough to insure a certain precision of statistics when the number of solute atoms is small. However, it should not be too high either, for then the simulation time will be too long. A simulation box containing 64 unit cells in each of the three space directions represents a good compromise, and was usually used in the simulations of Cu precipitation [12–14].

3.2.2. Influence of the parameters

In this section, we investigate the influence of the mixing energy, E_{mix}, the vacancy formation energy in pure bcc Cu, $E_{for}(V^{Cu})$, the binding energies between two Cu atoms, E_b(Cu–Cu), the binding energies between a vacancy and a Cu atom, E_b(V–Cu), and the interface energies, E_{int}. This study was done using the FISE model to simulate the ageing at 500 °C of an Fe–0.6%at.Cu alloy.

3.2.2.1. Mixing energy. Two values of the mixing energy were studied: 0.50 and 0.62 eV. The correct value of the mixing energy is essential for the precipitation as it gives the solubility limit of the system. A mixing energy of 0.50 eV leads to a solubility limit of 0.07at.% for Cu at 500 °C, which is close to the estimated experimental solubility limit (0.1 at.% [29]) while with a mixing energy of 0.62 eV, the solubility limit decreases to 0.01 at.%.

The influence of the value of the mixing energy on the time evolution of the microstructure is shown in Fig. 5. The values of the main parameters used for these simulations are in Table 3. As expected, the cluster growth is too slow when the value of the mixing energy is high (0.62 eV) (Fig. 5(a)). The growth exponent equals only 0.21, whereas the time evolution of the mean radius is well reproduced with the lowest value of the mixing energy (growth exponent close to 0.5). Another difference between these two KMC evolutions concerns the incubation time before the precipitate growth: this time is the longest with the lowest mixing energy. This tendency is in agreement with the work of Soisson and Martin [22]. Moreover, as was also expected, the numerical density of Cu precipitates, before decreasing, is three times higher with the high mixing energy than with the low one (Fig. 5(b)). The numerical density obtained with the highest mixing energy (6×10^{24} m^{-3}) is thus too high compared to the experimental value, which is around 10^{23} m^{-3}. One can thus conclude that the low mixing energy (0.50 eV) reproduces better the experimental growth kinetics of Cu precipitates after 3 h of thermal ageing. This comparison however is qualitative, because in the tomographic atom probe, precipitates are accounted for only when they contain more than 10 atoms. Furthermore, because of the efficiency, which is around 50%, this corresponds to precipitates containing in reality 20 atoms. If this had been taken into account in our simulations, rather than considering all clusters of size larger than four atoms, the calculated density would be much lower. The high mixing energy leads to the formation of too many precipitates, with a growth kinetics too slow. Also worth noting, the small differences between the first neighbour Cu–Cu binding energy from one set of parameter to the other one, cannot be responsible for the major difference in the evolution kinetics of the microstructure exhibited in Fig. 5.

Differences between the interfacial energies also exist because of the trivial dependence of the pair interaction parameters and the mixing energies.

Table 3
Values of some properties, important for the precipitation, used to show the influence of the mixing energy on the growth stage

	Set 1	Set 2
E_{mix}(Cu → Fe) (eV)	**0.50**	**0.62**
$E_b^{(1)}$(Cu–Cu) (eV)	0.14	0.14
$E_b^{(2)}$(Cu–Cu) (eV)	−0.02	0.02
E_{int}(100) (mJ/m^2)	504	581
E_{int}(110) (mJ/m^2)	329	438

3.2.2.2. Vacancy formation energy. The relaxed vacancy formation energy in bcc Cu metal cannot be obtained by ab initio calculations as the structure is unstable. This parameter has thus to be adjusted. Its influence was studied for values up to the vacancy formation energy in bcc Fe. For each value of the vacancy formation energy, the first nearest neighbour vacancy–Cu binding energy was kept equal to 0.07 eV, which led to the modification of the second nearest neighbour V–Cu binding energy. The values of the main properties obtained with three different values of the vacancy formation energy appear in Table 4. The microstructure evolutions versus time are shown in Fig. 6. The growth kinetics (Fig. 6(a)) is slightly accelerated when the vacancy formation energy in pure bcc Cu is increased. The kinetics obtained with the lowest value (set 3) looks slightly better. A low vacancy formation energy in bcc Cu means that a vacancy can be created easily in a Cu environment. Consequently, the smaller this value, the stronger the trapping of the vacancy in Cu clusters. Nevertheless, as the time is not incremented as soon as the vacancy is surrounded by two Cu atoms, the effect of the value of the vacancy formation energy in bcc copper is considerably reduced. The slight differences observed in the kinetics come thus from the differences in the vacancy trapping time near one Cu atom. The numerical densities of the Cu clusters (Fig. 6(b)) are all of the same order of magnitude. They are all one order of magnitude too high until 3 h, after which time the agreement between experiment and simulation is much better.

Table 4
Values of some properties, important for the precipitation, used to study the influence on the growth stage of the vacancy formation energy in bcc Cu

	Set 3	Set 1	Set 4
E_{mix}(Cu → Fe) (eV)	0.50	0.50	0.50
$E_{for}(V^{Cu})$ (eV)	**1.2**	**1.6**	**2.0**
$E_b^{(1)}$(V–Cu) (eV)	0.07	0.07	0.07
$E_b^{(2)}$(V–Cu) (eV)	0.12	0.06	−0.01
$E_{int}(100)$ (mJ/m^2)	407	407	407
$E_{int}(110)$ (mJ/m^2)	397	397	397

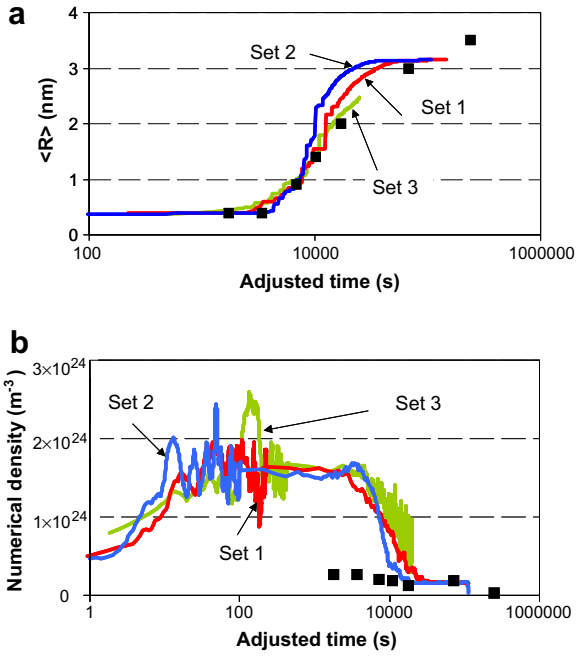

Fig. 6. Comparison of the kinetics obtained with different values of the vacancy formation energy in pure bcc Cu. The black filled squares are the experimental data. (a) Evolution of the Cu cluster mean radius. (b) Evolution of the numerical density of the Cu clusters. One cluster in the simulation box corresponds to a numerical density of 1.6×10^{23} m^{-3}.

The strongest effect of the value of the vacancy formation energy in pure Cu is on the computer time consumed. Indeed when this value is too low, the vacancy remains trapped in Cu clusters for the bulk of the simulation, during which time is not incremented. Thus, to reach the same ageing time, many more MC steps have to be performed. For example, 1.432×10^{11} MC steps were performed with the vacancy formation energy of 1.2 eV whereas only 6.55×10^9 MC steps were done with the value of 1.6 eV to simulate 3 h of ageing. Consequently, the vacancy formation energy should not be too low – 1.6 eV seems to be a good compromise.

3.2.2.3. First nearest neighbour Cu–Cu binding energy. The influence of the values of the first nearest neighbour Cu–Cu binding energy has been studied for both the low (0.50 eV) and the high (0.62 eV) mixing energy. This parameter could be important for the precipitation as it could accelerate the formation of Cu–Cu bonds and stabilize Cu clusters. The main values of each set of parameters studied are given in Table 5. The comparisons of the microstructural evolution kinetics of the FeCu system are shown in Fig. 7. With both mixing energies, the Cu cluster mean radius evolutions are similar in the first stages of thermal ageing. After 4 h of thermal ageing, with the low mixing energy, the curve obtained with the high first nearest neighbour Cu–Cu binding energy begins to saturate. A similar behaviour occurred after 160 h of thermal ageing with the high mixing energy. In each case, the maximal numerical density of Cu precipitates is three times higher when the Cu–Cu binding energy is high, which results in a simulated density that is too high compared to the experimental one. Thus, the high Cu–Cu binding energy enhances the

Table 5
Values of some properties, important for the precipitation, used to study the effect of the Cu–Cu binding energy

	Low mixing energy		High mixing energy	
	Set 1	Set 5	Set 2	Set 6
E_{mix}(Cu → Fe) (eV)	0.50	0.50	0.62	0.62
$E_b^{(1)}$(Cu–Cu) (eV)	**0.065**	**0.14**	**0.08**	**0.14**
$E_b^{(2)}$(Cu–Cu) (eV)	0.08	−0.02	0.1	0.02
$E_{int}(100)$ (mJ/m^2)	407	504	504	581
$E_{int}(110)$ (mJ/m^2)	397	329	493	438

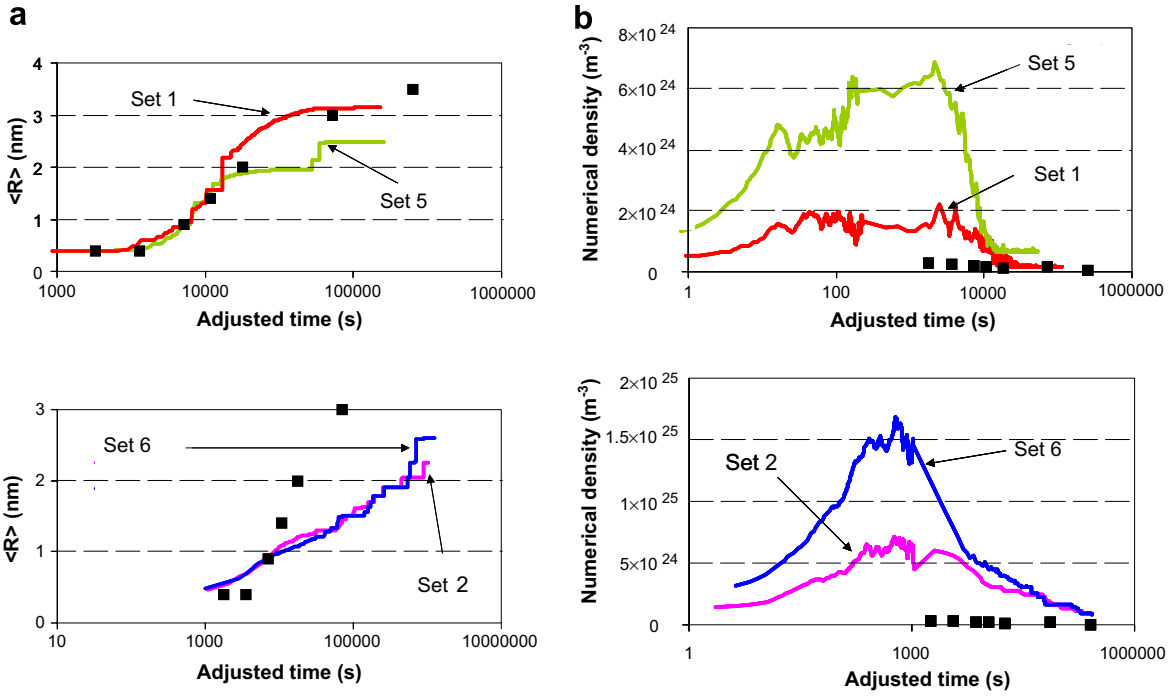

Fig. 7. Comparison of the kinetics obtained with different values of the first nearest neighbour Cu–Cu binding energy. For the graphs on the top, the mixing energy equal 0.50 eV and it equals 0.62 eV for the graphs on the bottom. The parameter sets used are collected in Table 5. The black filled squares are the experimental data. (a) Evolution of the Cu cluster mean radius. (b) Evolution of the numerical density of the Cu clusters. One cluster in the simulation box corresponds to a numerical density of 1.6×10^{23} m^{-3}.

tendency for Cu atoms to precipitate without modifying the mean size of the Cu clusters, at least until a certain thermal ageing time. At a given time, a greater amount of Cu has precipitated with a higher Cu–Cu binding energy. The saturations, observed on the evolution kinetics of the Cu cluster mean radius, appear, in each case, more rapidly when the Cu–Cu binding energy is high. Note that these saturations appear instead of the expected $t^{1/3}$ coalescence law, meaning that coalescence is not well reproduced in our systems. This process exists, but it is much too slow, perhaps because the Cu precipitates are too stable due to the values of the Cu–Cu binding energies and of the interface energies.

If one compares the microstructures obtained with parameter set number 5 with the low mixing energy and parameter set number 2 with the high mixing energy, it appears that the growth kinetics of the Cu precipitates are different but that their numerical densities are similar. Thus, for the numerical density, the effect of the mixing energy and of the first nearest neighbour Cu–Cu binding energy seems to be equivalent.

3.2.2.4. V–Cu binding energy. The influence of the first nearest neighbour V–Cu binding energy has been studied for a low (0.07 eV) and a high (0.14 eV) value. The important energies of the two parameter sets obtained with these two values of the V–Cu binding energy are collected in Table 6 and the evolution kinetics are shown in Fig. 8. Again, it appears that the numerical densities obtained are similar while the Cu cluster mean radius evolutions differ. Indeed, with the high V–Cu binding energy, the incubation time before the cluster growth is longer, followed by a faster cluster growth than in the case of the low first nearest neighbour V–Cu binding energy. These different behaviours arise from the vacancy efficiency for forming clusters. For V–nCu complexes, with n higher than 2, two binding energy calculations have been performed. First, we have determined the binding energy between a first nearest neighbour V–Cu pair and a $(n-1)$Cu cluster, E_b[(V–Cu)–$(n-1)$Cu]. Second, we have calculated the binding energy of a vacancy first nearest neighbour of a nCu cluster, E_b[V–nCu]. The two sets of calculations were done with the two parameter sets in Table 6. For both parameter sets, the differences E_b[(V–Cu)–$(n-1)$Cu] – E_b[V–nCu] were calculated and compared to each other. Whatever the cluster size, the values obtained with parameter set 1 are always

Table 6
Values of some properties, important for the precipitation, used to show the influence of the first nearest neighbour V–Cu binding energy

	Set 1	Set 7
$E_b^{(1)}$(V–Cu) (eV)	**0.07**	**0.14**
$E_b^{(2)}$(V–Cu) (eV)	0.06	0.05
E_{mix}(Cu → Fe) (eV)	0.50	0.50
$E_b^{(1)}$(Cu–Cu) (eV)	0.07	0.07
$E_b^{(2)}$(Cu–Cu) (eV)	0.08	0.08
E_{int}(100) (mJ/m^2)	407	407
E_{int}(110) (mJ/m^2)	397	397

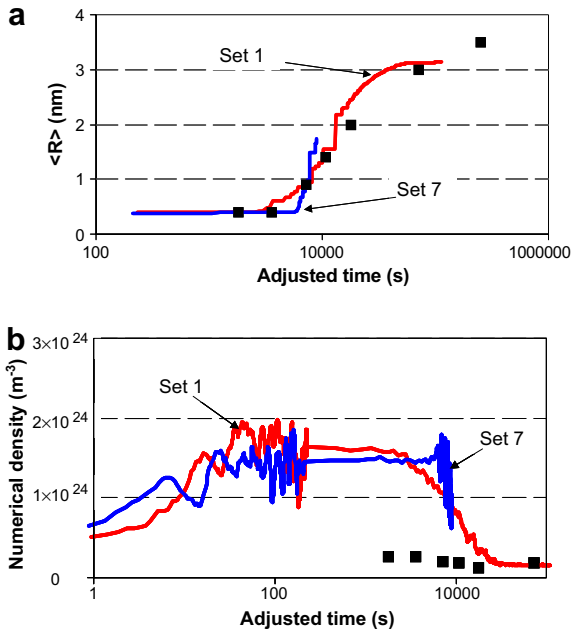

Fig. 8. Comparison of the kinetics obtained with different values of the first nearest neighbour V–Cu binding energy. The black filled squares are the experimental data. (a) Evolutions of the Cu cluster mean radius. (b) Evolutions of the numerical density of the Cu clusters. One cluster in the simulation box corresponds to a numerical density of 1.6×10^{23} m^{-3}.

higher than those obtained with parameter set 7. The difference is constant and equals 0.07 eV, which corresponds to the difference between the 2 first nearest neighbour V–Cu binding energies, the Cu–Cu binding energies being the same in the two parameter sets. The difference that we have calculated is important for the precipitation since the higher it is, the most difficult it is for a vacancy to jump from a precipitate, and so the less efficient the vacancy is for the precipitation. Moreover, if the vacancy is first nearest neighbour of only one Cu atom of the precipitates, time is incremented. Consequently, the vacancy is less efficient for the Cu precipitation with parameter set 1, that is why the cluster growth is slower with this parameter set.

3.2.2.5. Interface energy. The influence of the interface energies is difficult to investigate with our model. Indeed, the set of equations (Eqs. (6)–(12)) we used leads to a decrease of the interfacial energy along the (1 1 0) plane when the interface energy along the (1 0 0) plane is increased and vice versa. Furthermore, modifying an interface energy by a large amount leads to a big modification of the Cu–Cu binding energies which can become quite high. This effect can be seen in Table 7 in which two values of the (1 1 0) interface energy are presented. Consequently, it is not an easy task to isolate the effects of the changes of the interface energies. Nevertheless, the kinetics obtained with the parameter sets of Table 7 are shown in Fig. 9. The Cu cluster mean radius evolution is considerably slowed down when the (1 1 0) interface energy is the lowest, while the cluster density increases by more than one order

Table 7
Values of some properties, important for the precipitation, used to show the influence of the interface energies on the growth stage

	Set 1	Set 8
E_{mix}(Cu → Fe) (eV)	0.50	0.50
$E_b^{(1)}$(Cu–Cu) (eV)	0.07	0.28
$E_b^{(2)}$(Cu–Cu) (eV)	0.08	−0.20
E_{int}(1 0 0) (mJ/m^2)	**407**	**678**
E_{int}(1 1 0) (mJ/m^2)	**397**	**205**

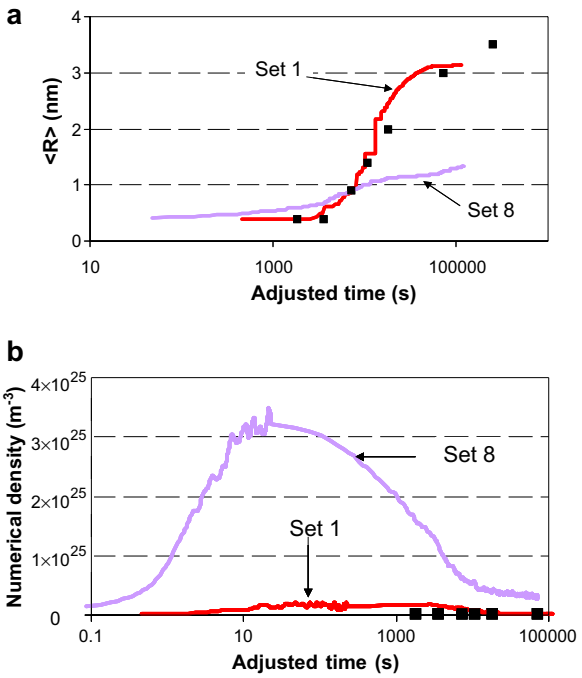

Fig. 9. Comparison of the kinetics obtained with different values of interface energies (Table 7). The black filled squares are the experimental data. (a) Evolution of the Cu cluster mean radius. (b) Evolution of the numerical density of the Cu clusters. One cluster in the simulation box corresponds to a numerical density of 1.6×10^{23} m^{-3}.

of magnitude. This indicates that for this value of the (1 1 0) interface energy more numerous but smaller precipitates are formed. These effects certainly arise because of the very high value of the first nearest neighbour Cu–Cu binding energy as was seen previously. It was not possible to study the effect of these parameters for a high decrease of the (1 0 0) interface energy and a high increase of the (1 1 0) one since it led to a negative first nearest neighbour Cu–Cu binding energy, which prevents Cu precipitation.

3.2.3. Final comparison of all the models

We now compare the different models [12–14] for the ageing of the Fe–0.6at.%Cu alloy at 500 °C and discuss the results in the light of the previous parametric study.

The evolutions of the precipitate mean radius and of their numerical density with ageing time are shown in Fig. 10. The time evolution of these two properties obtained with the FISE and the CBM2 methods combined with our parameter set and with the CBM1 method used

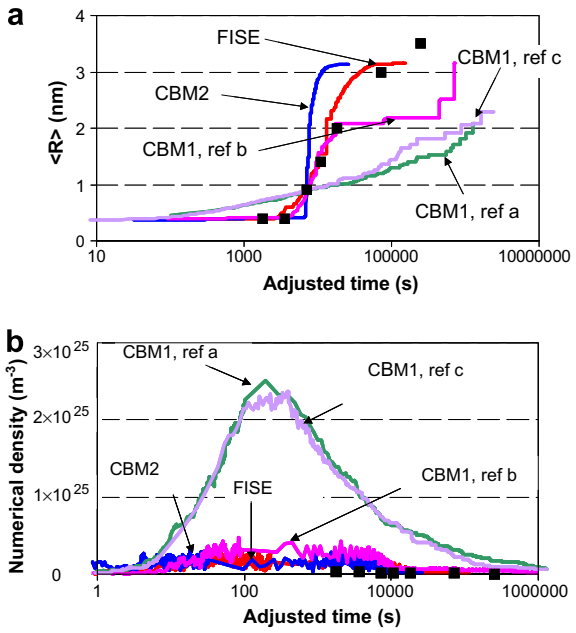

Fig. 10. Comparison of the evolution kinetics obtained for an Fe–0.6 at.%Cu alloy aged at 500 °C with the three models presented in this paper and the associated parameters (Table 1). The black filled squares are the experimental data. (a) Evolution of the Cu cluster mean radius. (b) Evolution of the numerical density of the Cu clusters. One cluster in the simulation box corresponds to a numerical density of 1.6×10^{23} m^{-3}.

with the parameter sets of [12–14] are compared. The FISE method used with our parameter set gives a time evolution of the precipitate mean radius in very good agreement with the experimental one until 17 h of thermal ageing. The kinetics obtained with the combination of our parameters and the CBM2 method is too fast, with a growth exponent of about 1. With the CBM1 method, the kinetics obtained with the parameters of Schmauder and Binkele [14] follows very well the experiments before reaching a plateau after around 10 h of thermal ageing. With this same method, the evolutions obtained both by Le Bouar and Soisson [13] and by Soisson et al. [12] appear to be too slow compared to the experimental one as the growth exponents equal respectively 0.14 and 0.16. Moreover, the numerical densities of the Cu precipitates obtained by [12,13] are the highest, by almost one order of magnitude, which leads them far from the experimental value estimated to be between 1×10^{23} and 3×10^{23} m^{-3}. From the parametric study, these tendencies can be explained by the values of both the mixing energy (a too high value leading to a too high supersaturation) and the Cu–Cu binding energies. Indeed, for [12,13] these values are very high while they are low for [14] as well as in our parameter set.

To complete this study, we have studied the impact of the parameter values on the vacancy migration energy. For each parameter set, the migration energy of a vacancy in the vicinity of a Cu atom has been determined for all possible jumps and compared. More precisely, for the configuration in which a Cu atom is first nearest neighbour of a vacancy in an iron matrix, the energetic barriers (one towards the Cu atom and the others towards Fe atoms) that the vacancy has to overcome as well as the energetic barriers of the reverse jumps have been determined and collected in Fig. 11. It appears clearly that for Le Bouar and Soisson [13] and for Soisson et al. [12], contrary to the other cases, the barriers that the vacancy has to overcome to jump towards the Cu atom are largely lower than all the other ones. As a result, the vacancy will be easily trapped by Cu, and the precipitation process will be inhibited. Trapping will also occur when the vacancy is first nearest neighbour of a Cu cluster but in this case, as explained previously, time is not incremented. The values of these barriers show how the 'macroscopic' parameterisation with the mixing energy can influence the microscopic evolution.

Another important parameter in the MC simulations is the calculation of the activation energy, since its values determine the vacancy diffusion path. Consequently, the three methods (FISE, CBM1 and CBM2), are now compared using exactly the same fitting parameters and the same simulation conditions. The parameterisation chosen was ours (Table 1, column 1). The precipitation kinetics obtained with each model for the 500 °C thermal ageing of the Fe–0.6 at.%Cu alloy appear along with the available experimental results in Fig. 12. The kinetics obtained with the FISE and the CBM1 models are very similar. The one obtained with the CBM2 model is different as the incubation time, before the growth phase, is longer and the growth kinetics faster. These differences can not come from the parameterisation and thus arise from the differences observed about the migration barriers. Indeed, changing the activation energy means changing the migration energy.

3.2.4. Temperature effect

MC parameters have been studied on precipitation for only one temperature. As one of the main purposes of the MC codes is to reproduce the temperature effect, we investigate the ability of the models to reproduce the recent results of Perez et al. [29] on an Fe–1.4 wt%Cu alloy aged at 500 °C and 600 °C.

3.2.4.1. Advancement factor. Rather than determining the Cu clusters' numerical density, Perez et al. [29] determined the precipitation advancement factor of the Fe–1.4 wt%Cu alloy aged at 500 °C and 600 °C. The precipitation advancement factors obtained with the FISE method combined with our parameters as well as with the CBM1 model combined with the parameters of [12–14] are given in Fig. 13 for 500 °C and 600 °C. For each series of curves, the multiplying factor used to adjust the time rescaled first with the Eqs. (19) and (21) is the same for the two temperatures. It has been determined from the advancement factor obtained at 500 °C. Globally, at 500 °C, the simulated advancement factors are in quite good agreement with the experimental one, those of Le Bouar and Soisson [13] and of Soisson et al. [12] being slightly the best ones. However, at 600 °C, the agreement is no longer as good because

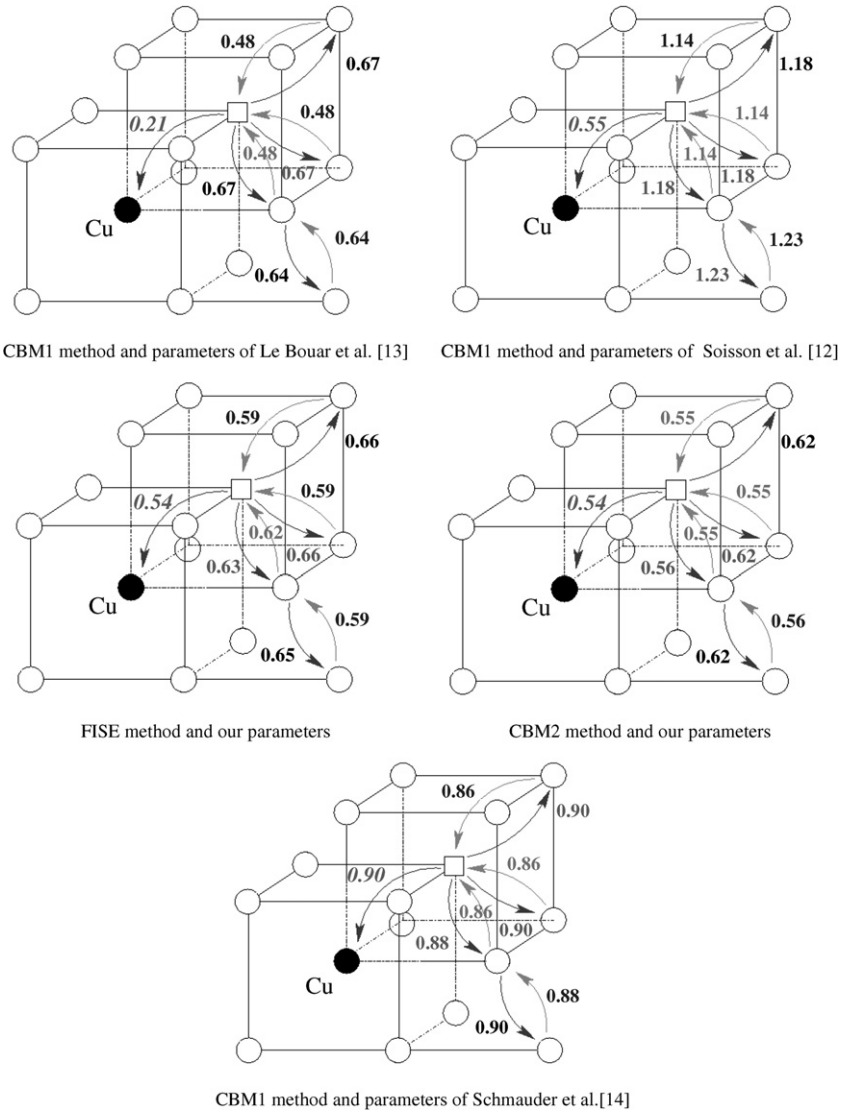

Fig. 11. Vacancy migration energies (in eV) when the vacancy is first nearest neighbour of a Cu atom for the three methods developed with their original parameters. The migration energies of the inverse jumps are also written. The vacancy is represented by the white square, the Cu atom by the black circle and the Fe atoms by the white circles.

the curves obtained are shifted towards shorter times compared to the experimental curve. Moreover, our parameters and those of Schmauder and Binkele [14] lead to curves whose slopes are too stiff. The parameters of Soisson et al. [12] and of Le Bouar and Soisson [13], on the other hand, lead to curves with very good tendencies. Thus, all models exhibit a temperature effect, however this effect does not always correspond exactly to the experimental one.

3.2.4.2. Evolution kinetics of the Cu cluster mean radius. The evolution kinetics of the Cu cluster mean radius formed in the Fe–1.4 wt%Cu alloy aged at 500 °C and 600 °C obtained with the FISE model combined with our parameters and with the CBM1 model associated with the parameters of Soisson et al. [12], Le Bouar and Soisson [13] and of Schmauder and Binkele [14] appear in Fig. 14. For each series of curves obtained with one of the parameter sets, time was adjusted with the same multiplying factor, determined previously from the advancement factor evolution at 500 °C (Fig. 14). At 500 °C, the mean radius evolutions are all too slow, but the one obtained with our parameters is the closest to the experimental kinetics, and follows it very well until 3.5 h of thermal ageing. At 600 °C, the kinetics are not correct either. Those obtained with the parameters of Soisson et al. [12] and of Le Bouar and Soisson [13] are still too slow. With our parameters, the growth begins slightly too early but the curve tendency is quite good (a simple modification of the time factor (translation of the curve in time) can lead to a good description of the time evolution of R). The curve obtained from the parameter set of Schmauder and Binkele [14] is also close to the experimental one before the slope changes. It seems thus to be difficult to obtain both a good advancement factor and a good cluster growth kinetics whatever the parameter set and the model used to determine the activation energy.

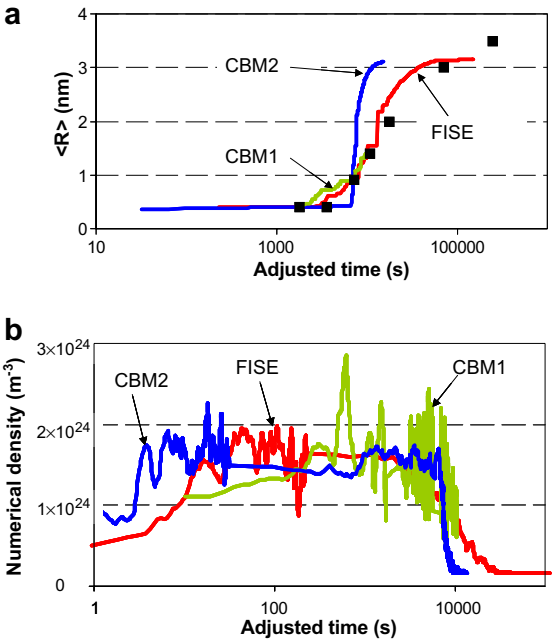

Fig. 12. Comparison of the kinetics obtained for the 500 °C thermal ageing of the Fe–0.6 at.%Cu alloy with the three different models presented used to determine the activation energy. The parameters used are ours (Table 1, column 1). The black filled squares are the experimental data. (a) Evolutions of the Cu cluster mean radius. (b) Evolutions of the numerical density of the Cu clusters. One cluster in the simulation box corresponds to a numerical density of 1.6×10^{23} m^{-3}.

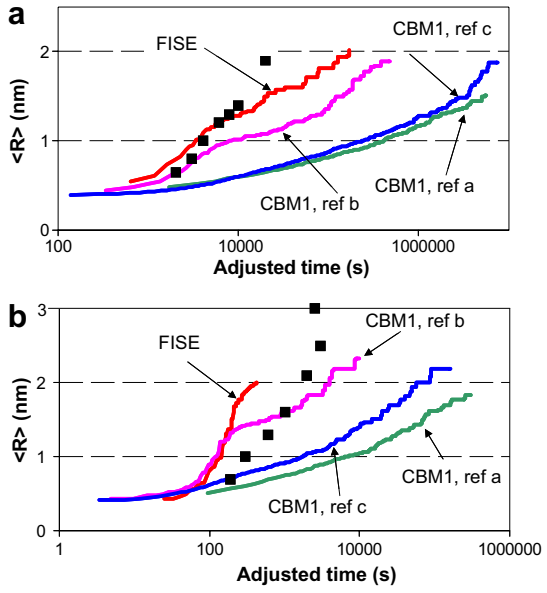

Fig. 13. Cu cluster mean radius evolutions as a function of time for an Fe–1.4 wt%Cu alloy aged at (a) 500 °C and (b) 600 °C. The curves obtained with the different methods and the associated parameters (Table 1) as well as the experimental kinetics [29] are compared. The black filled squares are the experimental data.

Indeed, for the advancement factor, the best tendencies are those of Le Bouar and Soisson [13] and of Soisson et al. [12], but their parameter sets give too slow cluster growth

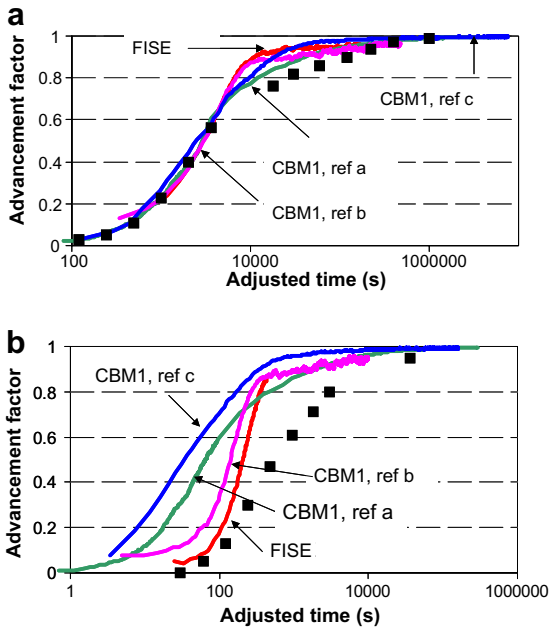

Fig. 14. Advancement factor evolutions as a function of time for an Fe–1.4 wt%Cu alloy aged at 500 and 600 °C. The curves obtained with the different methods and the associated parameters (Table 1) as well as the experimental kinetics [29] are compared. The black filled squares are the experimental data.

kinetics. Conversely, our parameters lead to correct Cu cluster growth kinetics but the corresponding advancement factors tend too rapidly until 1. This indicates that other corrections need maybe to be included in the data treatment to obtain a better agreement and shows that confronting data from simulations to experimental data is not a trivial task even in what appears to be a simple case.

These results show the necessity of validating a MC parameterisation on at least two microstructural parameters (Cu cluster size plus numerical density or Cu cluster size and advancement factor). Using only the advancement factor evolution is misleading, as for a given value of this parameter, the microstructure can be composed of either a great number of small clusters or a small number of big clusters.

None of the models reproduces accurately the temperature effects. This problem can be due to a bad evaluation of the vacancy formation energy, a too simplistic model and/or to the fact that our models apply for FeCu alloys of the highest purity, whereas in reality impurities such as carbon can have an influence on the kinetics, influence not taken into account in our models. Another discrepancy found with all the KMC methods investigated here is that the numerical densities simulated are always higher than the experimental ones. This may be due to the difficulty of defining whether an atom belongs to the solid solution or to a cluster. Furthermore, let us not forget that the tomographic atom probe efficiency of detected atoms is around 50%. This has not been taken into account in this work.

4. Conclusion

We have compared different kinetic Monte Carlo methods used to simulate the precipitation of the FeCu system. A parametric study indicates that, as expected, the mixing energy is the most important parameter for the precipitation kinetics as it determines the solubility limit of the system as well as the driving force of the precipitation of the Cu clusters. The Cu–Cu binding energy and the interface energies are also important parameters for the precipitation since they can enhance or hinder the precipitation of Cu atoms. Our study also indicates the importance of validating the MC simulations using at least two microstructural parameters (the Cu cluster mean size, their numerical density or the advancement factor).

Acknowledgements

The authors wish to thank Y. Bréchet for stimulating discussions about the Cu precipitation. This work has been performed within the European PERFECT project (FI6O-CT-2003-508840) which has sponsored this study. This research has been done using the CRI supercomputer of the USTL supported by the Fonds Européens de Développement Régional, the CEA CCRT supercomputers in the framework of an EDF-CEA contract as well as the by the computer-time Grants 2015014 of the Centre de Ressources Informatiques de Haute Normandie (CRIHAN).

References

[1] E. Hornbogen, R.C. Glenn, Trans. Metall. Soc. AIME 218 (1960) 1064.
[2] M.K. Miller, B.D. Wirth, G.R. Odette, Mater. Sci. Eng. A 353 (2003) 133.
[3] J.T. Buswell, W.J. Phythian, R.J. McElroy, S. Dumbill, P.H.N. Ray, J. Mace, R.N. Sinclair, J. Nucl. Mater. 225 (1995) 196.
[4] B.D. Wirth, PhD thesis, University of California, Santa Barbara, 1995.
[5] P. Auger, P. Pareige, M. Akamatsu, .J.C. Van Duysen, J. Nucl. Mater. 211 (1994) 194.
[6] M.K. Miller, P. Pareige, Mater. Res. Soc. Symp. 650 (2001) R6.1.1.
[7] B. Radiguet, PhD thesis, Université de Rouen, 2004.
[8] K. Osamura, H. Okuda, M. Takashima, K. Asano, M. Furusaka, Mater. Trans., JIM 34 (1993) 305.
[9] S.R. Goodman, S.S. Brenner, J.R. Low, Metall. Trans. 4 (1973) 2371.
[10] M.H. Mathon, A. Barbu, F. Dunstetter, F. Maury, N. Lorenzelli, C.H. de Novion, J. Nucl. Mater. 245 (1997) 22.
[11] A. Hardouin Duparc, C. Moingeon, N. Smetniansky-de-Grande, A. Barbu, J. Nucl. Mater. 302 (2002) 143.
[12] F. Soisson, A. Barbu, G. Martin, Acta Mater. 44 (1996) 3789.
[13] Y. Le Bouar, F. Soisson, Phys. Rev. B 65 (2002) 094103.
[14] S. Schmauder, P. Binkele, Comput. Mater. Sci. 24 (2002) 42.
[15] C. Domain, C.S. Becquart, J.C. Van Duysen, Mater. Res. Soc. Symp. Proc. 650 (2001) R3.25.1.
[16] I.M. Lifshitz, V.V. Slyozov, J. Phys. Chem. Solids 19 (1961) 25.
[17] C. Wagner, Z. Electrochem. 65 (1961) 581.
[18] G. Kresse, J. Hafner, Phys. Rev. B 47 (1993) 558;
G. Kresse, J. Hafner, Phys. Rev. B 49 (1994) 14251.
[19] G. Kresse, J. Furthmüller, Comput. Mater. Sci. 6 (1996) 15.
[20] C. Domain, C.S. Becquart, Phys. Rev. B 65 (2002) 024103.
[21] W.M. Young, E.W. Elcock, Proc. Phys. Soc. 89 (1966) 735.
[22] F. Soisson, G. Martin, Phys. Rev. B 62 (2000) 203.
[23] E. Vincent, C.S. Becquart, C. Domain, J. Nucl. Mater. 351 (2006) 88.
[24] C. Domain, C.S. Becquart, J.C. Van Duysen, Mater. Res. Soc. Symp. Proc. 650 (2001) R3.25.1.
[25] B.D. Wirth, G.R. Odette, Mater. Res. Soc. Symp. Proc. 540 (1999) 637.
[26] C. Kittel, Introduction to Solid State Physics, 6th Ed., Wiley, New York, 1987.
[27] E. Vincent, C.S. Becquart, C. Domain, Nucl. Instrum. and Meth. B 255 (2007) 78.
[28] N. Metropolis, A.W. Rosenbluth, M.N. Rosenbluth, A.H. Teller, E. Teller, J. Chem. Phys. 21 (1953) 1087.
[29] M. Perez, F. Perrard, V. Massardier, X. Kleber, A. Deschamps, H. de Monestrol, P. Pareige, G. Covarel, Philos. Mag. 85 (2005) 2197.
[30] M. Akamatsu, PhD thesis, Paris XI Orsay, 1994.
[31] G.M. Worrall, J.T. Buswell, C.A. English, M.G. Hetherington, G.D.W. Smith, J. Nucl. Mater. 148 (1987) 107.
[32] M. Charleux, F. Livet, F. Bley, F. Louchet, Y. Bréchet, Philos. Mag. A 73 (1996) 883.
[33] C. Zener, J. Appl. Phys. 20 (1949) 950.
[34] F. Maury, N. Lorenzelli, M.H. Mathon, C.H. de Novion, P. Lagarde, J. Phys.: Condens. Mater. 6 (1994) 569.
[35] P.J. Othen, M.L. Jenkins, G.D.W. Smith, W.J. Phythian, Philos. Mag. Lett. 64 (1991) 383.
[36] P.J. Othen, M.L. Jenkins, G.D.W. Smith, Philos. Mag. A 70 (1994) 1.
[37] K. Osamura, H. Okuda, K. Asano, M. Furusaka, K. Kishida, F. Kurosawa, R. Uemori, ISIJ Int. 34 (1994) 346.
[38] M.H. Mathon, PhD thesis, Université d'Orsay, Paris-Sud, 1995.